Addition to the known diversity of Chinese freshwater planarians: integrative description of a new species of *Dugesia* Girard, 1850 (Platyhelminthes, Tricladida, Dugesiidae)

Yi Liu[1], Xiao-Yu Song[1,2], Zhong-Yin Sun[1], Wei-Xuan Li[3], Ronald Sluys[4], Shuang-Fei Li[1], An-Tai Wang[1]

1 *Shenzhen Key Laboratory of Marine Bioresource and Eco-environmental Science, College of Life Sciences and Oceanography, Shenzhen University, Shenzhen, Guangdong, China*

2 *School of Urban Planning and Design, Shenzhen Graduate School, Peking University, Shenzhen, China*

3 *State Key Laboratory of Protein and Plant Gene Research, Center for Bioinformatics, School of Life Sciences, Peking University, Beijing, China*

4 *Naturalis Biodiversity Center, P.O. Box 9517, Leiden, 2300 RA, Netherlands*

https://zoobank.org/E8B38FE7-A904-43D2-8024-EE0745E415C7

Corresponding author: Shuang-Fei Li (sfli@szu.edu.cn)

Abstract

The present paper describes a new species of freshwater flatworm of the genus *Dugesia* from Guizhou province, China, based on an integrative approach, combining morphological, histological and molecular information. This new species, *Dugesia gemmulata* Sun & Wang, sp. nov., is characterized by the ventral part of the most posterior section of the bursal canal being provided with a voluminous, ellipsoidal muscular swelling; sac- or egg-shaped seminal vesicle situated near the ventral body surface in anterior portion of the penis bulb; postero-dorsal wall of seminal vesicle communicating with a narrow duct that first runs almost vertically but then shows a postero-dorsally directed loop before connecting with a small diaphragm; an ejaculatory duct opening terminally or subterminally; an asymmetrical penis papilla, with its dorsal lip being provided with a bump; oviducts opening asymmetrically into female copulatory apparatus, with the left oviduct opening into the common atrium and the right oviduct opening into the vaginal section of the bursal canal. Molecular phylogenetic analyses revealed that the new species belongs to a clade comprising species from the Australasian and Oriental regions, while it shares a sister-group relationship with *D. umbonata* Song & Wang, 2020, a species characterized by a muscular swelling on the dorsal side of its bursal canal.

Key Words

Introduction

Freshwater planarians of the genus *Dugesia* Girard, 1850 (Platyhelminthes, Tricladida, Dugesiidae) currently comprise about 100 nominal species distributed in a large part of the Old World and Australia (Sluys and Riutort 2018: fig. 13B). For a long period of time, *Dugesia japonica* Ichikawa & Kawakatsu, 1964 was the only known *Dugesia* species from mainland China (cf. Kawakatsu et al. 1995). However, over the past few years renewed attention paid to this group of animals has rapidly increased the number of Chinese *Dugesia* by seven more species, viz., *D. sinensis* Chen & Wang, 2015, *D. umbonata* Song & Wang, 2020, *D. semiglobosa* Chen & Dong, 2021, *D. majuscula* Chen & Dong, 2021, *D. circumcisa* Chen & Dong, 2021, *D. verrucula* Chen & Dong, 2021, and *D. constrictiva* Chen & Dong, 2022 (Chen et al. 2015; Song et al. 2020; Wang et al. 2021a, b, 2022).

In the present study we provide an integrative description of another new species of *Dugesia*, which was collected from Guizhou Province located at a plateau in the southwest of China, on the basis of morphological, histological and molecular data.

Materials and methods

Sample collection and culturing

The specimens were collected in a rural streamlet at an altitude of about 1,400 m in Qingzhen City, Guizhou Province, China (26°33.83'N, 106°13.65'E; Fig. 1). The animals were collected from the underside of small pebbles in the riverbed and, thereafter, were transported to Shenzhen University. The animals were reared as described in Song et al. (2020). Only 15 specimens were collected at the beginning, none of which was sexually mature. During about two years of rearing under laboratory conditions, the animals multiplied by means of fission and, eventually, in total, about 30 specimens sexualised.

DNA extraction, amplification, sequencing and phylogenetic analysis

After starvation for three days, total DNA was extracted independently from three asexual fissiparous individuals, using the E.Z.N.A.™ Mollusc DNA Isolation Kit (Omega, Norcross, GA, USA). Cytochrome C oxidase subunit I (*COI*) gene was amplified by polymerase chain reaction (PCR), using forward primer *COI*F: GCT CAT GGT TTA RTW ATG ATG ATT TTY TT and reverse primer *COI*R: GWG CAA CAA CAT ART AAG TAT CAT (Chen et al. 2015). PCR was performed as follows: denaturation of 5 min at 94 °C, followed by 35 cycles of 50 s at 94 °C, 45 s at 5 °C, 50 s at 7 °C and finally 7 min extension at 72 °C (Chen et al. 2015). DNA sequences were determined by Sanger sequencing in Beijing Genomics Institution (BGI, Shenzhen, China) and by using the same primers as used for the amplification. All new sequences have been uploaded in GenBank, NCBI (Table 1).

Phylogenetic trees were generated on the basis of *COI* data of the following ingroup taxa: the new species *Dugesia gemmulata* Sun & Wang, sp. nov. (described below) and 41 other species of the genus *Dugesia* (Table 1). For outgroups, we used two other dugesiid taxa, viz., *Recurva postrema* Sluys & Solà, 2013 and *Schmidtea mediterranea* Benazzi et al., 1975. All sequences were downloaded from GenBank, NCBI (Table 1).

Methods and parameters for identification of open reading frames and substitution saturation assessment were the same as in Song et al. (2020). *COI* sequences were translated into amino acids, using genetic code 9 (echinoderm and flatworm mitochondrial genetic code), after which they were aligned by MUSCLE (Edgar 2004) in the TRANSLATOR X server (Abascal et al. 2010).

Regions of ambiguous alignments were excluded by GBLOCKS (Talavera and Castresana 2007), using the less stringent selection option (smaller final blocks, gap positions within the final blocks, and less strict flanking positions allowed). JMODELTEST 2.1.7 (Darriba et al. 2012) was used to estimate the best-fit evolution model for the Bayesian Inference method (BI); the GTR+I+G model was selected by applying the Akaike information criterion (AIC). MODELFINDER (online version: http://iqtree.cibiv.univie.ac.at/; accessed 18 Jan. 2022; Kalyaanamoorthy et al. 2017) was used to find the best-fit evolution model for the Maximum Likelihood method (ML); the GTR+F+I+G4 model was selected by applying the Bayesian Inference criterion (BIC).

Phylogenetic trees were constructed by ML and BI methods, using IQ-TREE 2.1.3 (Minh et al. 2020) and MR-BAYES 3.2.6 (Ronquist et al. 2012), respectively. For ML, ultrafast bootstrap analysis with 10,000 replications was used to assess the confidence level of the nodes (Hoang et al. 2018). For BI, the Markov Chain Monte Carlo (MCMC) algorithm was run for 7,000,000 generations in four simultaneous chains, sampling every 7,000 generations. In order to ensure that the chains had reached the stationary region, we terminated the analysis when the average standard deviation of split frequencies was consistently lower than 0.01; the first 25% of the generated trees were discarded as burn-in to obtain the consensus tree and posterior probability values. We checked the .*p* file of each run in TRACER v1.7.1 (Rambaut et al. 2018) to ensure that the effective sample size (ESS) values of each parameter were above 200.

Table 1. GenBank accession numbers of *COI* sequences used in the phylogenetic analyses.

Species	COI	Species	COI
Recurva postrema	KF308763	*D. gibberosa*	KY498857
Schmidtea mediterranea	JF837062	*D. gonocephala*	FJ646941, FJ646986
Dugesia aethiopica	KY498845	*D. hepta*	MK712639
D. afromontana	KY498846	*D. ilvana*	FJ646989, FJ646944
D. arcadia	KC006969	*D. improvisa*	KF308774
D. ariadnae	JN376142	*D. japonica*	AB618487
D. aurea	MK712632	*D. liguriensis*	MK712645
D. batuensis	KF907819	*D. majuscula*	MW533425
D. benazzii	FJ646977, FJ646933	*D. malickyi*	KF308750
D. bifida	KY498851	*D. naiadis*	KF308757
D. bijuga	MH119630	*D. notogaea*	FJ646993, FJ646945
D. circumcisa	MZ147041	*D. parasagitta*	KF308739
D. corbata	MK712637	*D. pustulata*	MH119631
D. constrictiva	MZ871766	*D. ryukyuensis*	AB618488
D. cretica	KC006974	*D. sagitta*	KC007006
D. damoae	KF308768	*D. semiglobosa*	MW525210
D. deharvengi	KF907820	*D. sicula*	KF308797
D. effusa	KF308780	*D. sigmoides*	KY498849
D. elegans	KC006985	*D. sinensis*	KP401592
D. etrusca	MK712651	*D. subtentaculata*	MK712561
D. gemmulata sequence 1	OL632201*	*D. umbonata*	MT176641
D. gemmulata sequence 2	OL632202*	*D. verrucula*	MZ147040
D. gemmulata sequence 3	OL632203*	*D. vilafarrei*	MK712648

*Sequences from this study.

Histology

Histological sections were made using three-day starved animals in the same procedure as described in Song et al. (2020). Histological sections were made at intervals of 6 μm. Specimens were stained in slightly modified Cason's Mallory-Heidenhain stain solution (see Yang et al. 2020). Hereafter, slides were mounted with neutral balsam (Shanghai Yuanye Biotechnology Co., Ltd.). Histological glass slides were deposited in the Institute of Zoology, Chinese Academy of Science (IZCAS), Beijing, China.

Abbreviations used in the figures

ag: auricular groove; **au**: auricle; **bc**: bursal canal; **ca**: common atrium; **cb**: copulatory bursa; **ceg**: cement glands; **cm**: circular muscle; **d**: diaphragm; **du**: duct; **e**: eye; **ed**: ejaculatory duct; **go**: gonopore; **ie**: inner epithelium; **lm**: longitudinal muscle; **lod**: left oviduct; **lvd**: left vas deferens; **ma**: male atrium; **ms**: muscular swelling; **od**: oviduct; **oe**: outer epithelium; **ov**: ovary; **pb**: penis bulb; **pg**: penis glands; **ph**: pharynx; **pp**: penis papilla; **rod**: right oviduct; **rvd**: right vas deferens; **sg**: shell glands; **sv**: seminal vesicle.

Results

Molecular phylogeny

The amplified sequences of the *COI* sequence had a length of approximately 900 base pairs (bp). After GBLOCKS processing, the *COI* dataset comprised 46 Operational Taxonomic Units (OTUs) and 762 bp in length. Nucleotide saturation analysis was conducted on the fully resolved sites only, while all three codon positions were included. The critical Iss.c values (Iss.cSym=0.717; Iss.cAsym=0.428) were both greater than the observed Iss values (0.141), suggesting little substitution saturation in our dataset (Xia et al. 2003).

The phylogenetic trees constructed by BI and ML methods have identical topologies (Fig. 2). Three individuals of *Dugesia gemmulata* cluster together with very high support values (1.00 posterior probability – pp; 100% bootstrap – bs; Fig. 2), while they share a sister-group relationship with *D. umbonata* Song & Wang, 2020 that is well supported (0.80 pp; 90% bs; Fig. 2). The clade comprising *D. gemmulata* and *D. umbonata* is sister to *D. japonica* Ichikawa & Kawakatsu, 1964 with high support (0.87 pp; 91% bs; Fig. 2), and together they cluster with *D. circumcisa* Chen & Dong, 2021 with 81% bs (Fig. 2). These four species together form a clade that shares a sister-group relationship (88% bs) with a clade composed of the two species *D. sinensis* Chen & Wang, 2015 and *D. semiglobosa* Chen & Dong, 2021 (Fig. 2). This clade of six species clusters with a clade of seven other species from Australian and Oriental regions (from

D. notogaea Sluys & Kawakatsu, 1998 to *D. majuscula* in Fig. 2) with 0.85 pp and 89% bs. This entire Australasian-Oriental clade is sister to a Western Palearctic clade (from *D. malickyi* De Vries, 1984 to *D. hepta* Pala et al., 1981 in Fig. 2). The major clade formed by the two sister-clades of the Australasian-Oriental regions and the Western Palearctic shares a sister-group relationship with two species from Cameroon (*D. bijuga* Harrath & Sluys, 2019 and *D. pustulata* Harrath & Sluys, 2019), while these two clades together are sister to a small clade of three species from Madagascar. The most basal clade in our tree is formed by a clade comprising four species from the Afrotropical and South-West Palearctic regions (from *D. naiadis* Sluys, 2013 to *D. sicula* Lepori, 1948 in Fig. 2).

Systematic Account

Order Tricladida Lang, 1884
Suborder Continenticola Carranza, Littlewood, Clough, Ruiz-Trillo, Baguñà & Riutort, 1998
Family Dugesiidae Ball, 1974
Genus *Dugesia* Girard, 1850

***Dugesia gemmulata* Sun & Wang, sp. nov.**
https://zoobank.org/4C439299-E70E-4421-98E9-6068C91A1423

Material examined. *Holotype*: IZCAS PLA-0101, a rural streamlet in Qingzhen City, Guizhou, China, 26°33.83'N, 106°13.65'E, 3 February 2018, coll. Zhong-Yin Sun, sagittal sections on 20 slides.

Paratypes: IZCAS PLA-0102, ibid., sagittal sections on 30 slides; IZCAS PLA-0103, ibid., horizontal sections on 18 slides.

Habitat. Specimens were collected from a rural streamlet (26°33.83'N, 106°13.65'E) at an altitude of about 1,400 m above sea level (a.s.l.) in Qingzhen City, Guizhou, China (Fig. 1A). The animals were collected from the underside of small pebbles in the riverbed (Fig. 1B, C), which had a water depth of 20–50 cm. Water temperature was about 19.9 °C, while air temperature was about 21.8 °C.

Diagnosis. *Dugesia gemmulata* is characterised by the following characters: ventral part of the most posterior section of the bursal canal, just anteriorly to its point of communication with the common atrium, provided with a voluminous, ellipsoidal muscular swelling; sac- or egg-shaped seminal vesicle situated near the ventral body surface in anterior portion of the penis bulb; postero-dorsal wall of seminal vesicle communicates with a narrow duct that first runs almost vertically but then shows a postero-dorsally directed loop before connecting with a small diaphragm; ejaculatory duct opening terminally or subterminally; penis papilla asymmetrical, with dorsal lip provided with a bump; oviducts opening asymmetrically into female copulatory apparatus, with the left oviduct opening into the common atrium and the right oviduct opening into the vaginal section of the bursal canal.
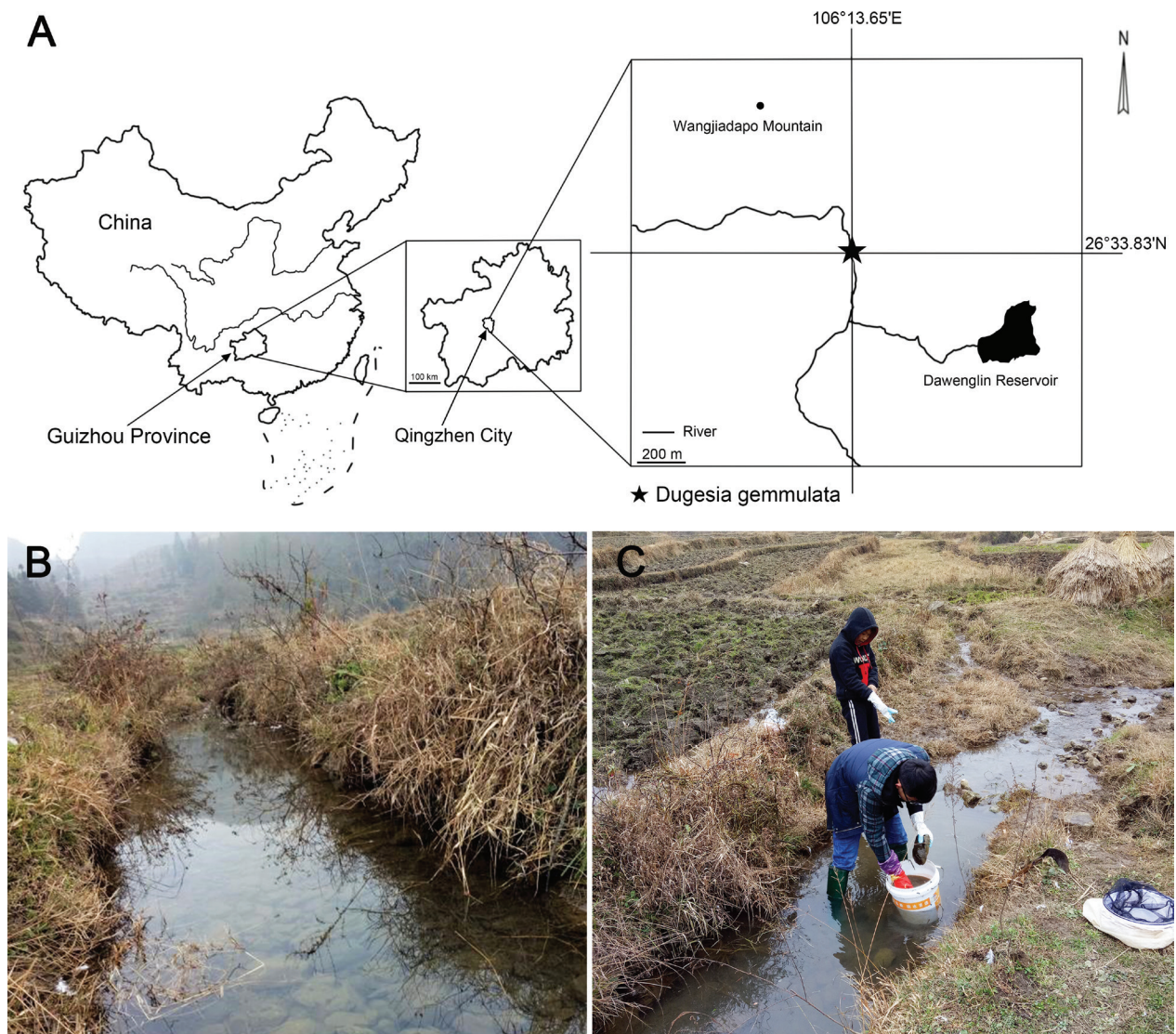
Figure 1. Locality and habitat of *Dugesia gemmulata*. **A.** Sampling locality in Qingzhen City, Guizhou, China; **B, C.** Habitat at sampling locality.

Etymology. The specific epithet is derived from the Latin *gemmula*, small bud, and alludes to the muscular swelling on the ventral wall of the bursal canal.

Description. Body size of live, sexualised specimens ranged from 16.12 to 22.75 mm in length and 1.93 to 2.87 mm in width (*n* = 3; Fig. 3A, B), while asexual specimens ranged from 5.12 to 8.31 mm in length and 0.91 to 1.32 mm in width (*n* = 3). Sexualised and asexual individuals exhibited no differences in appearance, except for the body size. The following measurements are based on sexualised individuals. At a distance varying between 0.46 mm and 0.56 mm from the anterior body margin, two eyes are present in the middle of the low-triangular head, situated in pigment-free patches (*n* = 3; Fig. 3C). Each kidney-shaped eyecup contains numerous retinal cells. Unpigmented auricular grooves are marginally placed just posteriorly to the blunt auricles (Fig. 3C).

Dorsal body surface with a brown ground colour, overlain with scattered black pigmentation and provided with a thin, pale median line that runs from anterior to the eyes to the tail end (Fig. 3A–C); ventral surface much paler than dorsal surface (Fig. 3D).

The cylindrical pharynx lies more or less in the middle of the body and measures about 1/7 of the total body length, i.e., about 2.07–2.77 mm in length and 0.16–0.32 mm in width (*n* = 3; Fig. 3A). The entire pharynx is covered with a nucleated epithelium (Fig. 4B). The outer epithelium of the pharynx is underlain by 1–3 subepithelial layers of circular muscles, followed by a thin layer of longitudinal muscle fibres (Fig. 4B). The inner pharynx epithelium, which is densely ciliated, is underlain by a thin subepithelial layer of longitudinal muscle fibres, followed by 3–5 layers of circular muscles (Fig. 4B). The mouth opening is located at a distance of about 1/3–1/2 of the body length, as measured from the posterior body margin; the mouth is situated at the posterior end of the pharyngeal cavity (*n* = 3; Fig. 3B).
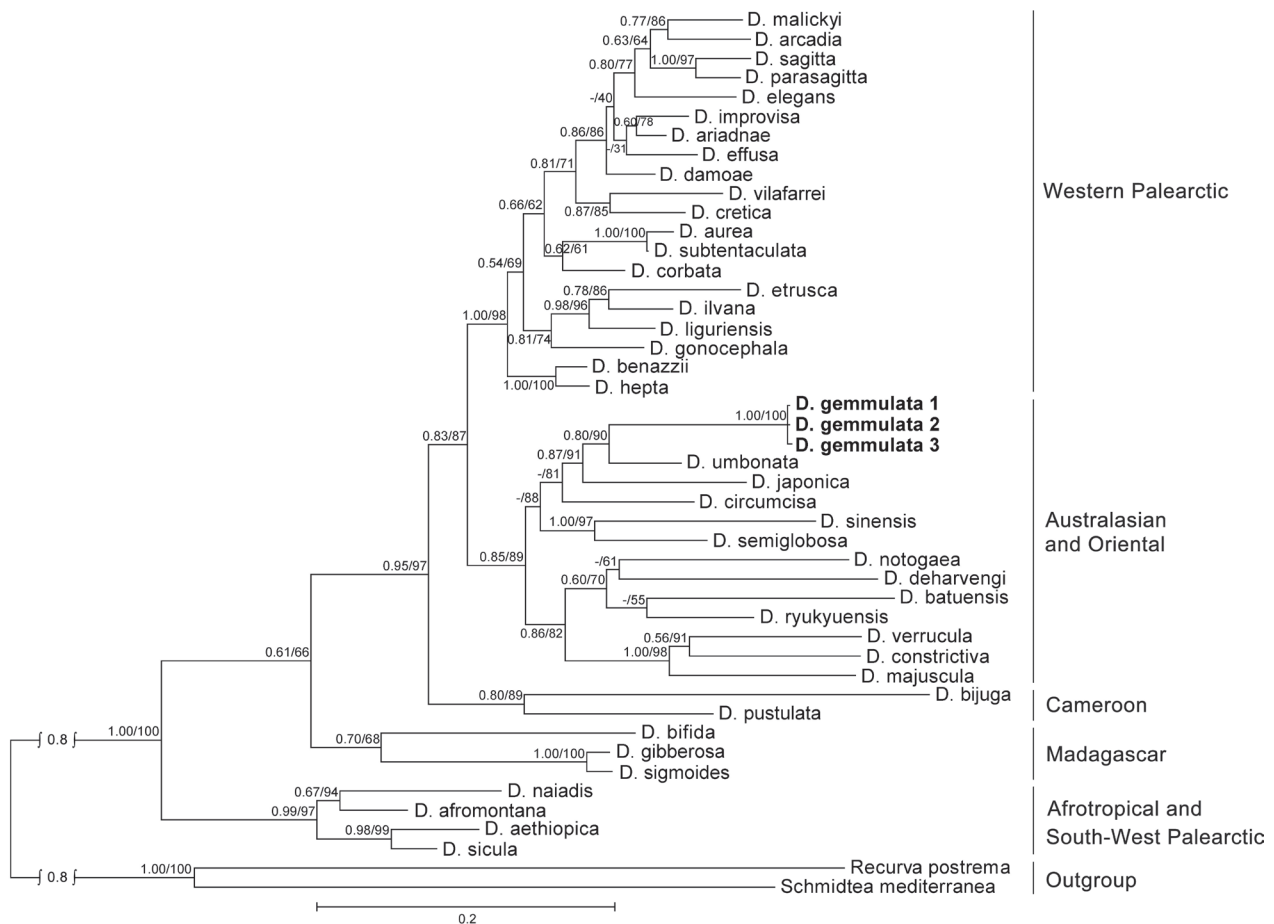
Figure 2. Maximum likelihood phylogenetic tree topology based on *COI* sequence. Numbers at nodes indicate support values (posterior probability/bootstrap). Scale bar: substitutions per site.

Testes could not be discerned. The large, elongated penis bulb consists of intermingled longitudinal and circular muscle fibres. The vasa deferentia open asymmetrically into the seminal vesicle, with the right vas deferens opening into the mid-anterior portion of the seminal vesicle in specimen PLA-0101 and into the mid-dorsal portion in specimen PLA-0102, while the left vas deferens opens into the postero-dorsal part of the seminal vesicle in specimen PLA-0101 and into the postero-ventral part in specimen PLA-0102 (Figs 4E, 5C). The sac- or egg-shaped seminal vesicle is situated near the ventral surface in the anterior portion of the penis bulb; it is lined with a nucleated epithelium and surrounded by 1–2 layers of longitudinal muscles (Figs 4C, E, 5A, C). From the postero-dorsal wall of the seminal vesicle arises a narrow duct, lined with a glandular, nucleated epithelium and surrounded by 1–3 layers of circular muscle fibres, which first runs almost vertically but then shows a postero-dorsally directed loop before connecting with a small diaphragm (Figs 4C, E, 5A, C).

The very small diaphragm is lined by a nucleated epithelium, which is underlain by 1–2 layers of circular muscle and is pierced by the openings of erythrophil penial glands (Figs 4C, E, 5A, C). The diaphragm leads to a broad ejaculatory duct, which is lined by an infranucleated epithelium that is underlain with 1–3 layers of circular muscle fibres (Figs 4C, E, 5A, C).

The ejaculatory duct runs more or less centrally through the penis papilla and opens subterminally through the ventral wall of the penis papilla in specimens PLA-0101 and PLA-0103, while in specimen PLA-0102 the ejaculatory duct runs a ventrally displaced course and opens at the tip of the papilla (Figs 4C, E, 5A, C). The penis papilla is asymmetrical, in that its dorsal lip is larger than the ventral one, while the former carries a bump (Figs 4C, E, 5A, C). The papilla is covered by a thin, nucleated epithelium, which is underlain by a layer of longitudinal muscles, followed by 2–3 layers of circular muscles, the latter being thicker at the base of penis papilla (Figs 4C, E, 5A, C).

The ovaries are hyperplasic, with several scattered masses distributed in the body region directly posterior to the brain, filling up the entire dorso-ventral space (Fig. 4A). The left oviduct arises from the mid-lateral section of the ovary, while the right duct arises from a more antero-lateral section of the ovary (Fig. 4A). From the ovaries, the oviducts, which are lined with an infranucleated epithelium, run backwards and continue their course on either side of the pharyngeal pocket (Figs 4F, 5D). Immediately posterior to the gonopore, the oviducts turn medially to open asymmetrically into the female copulatory
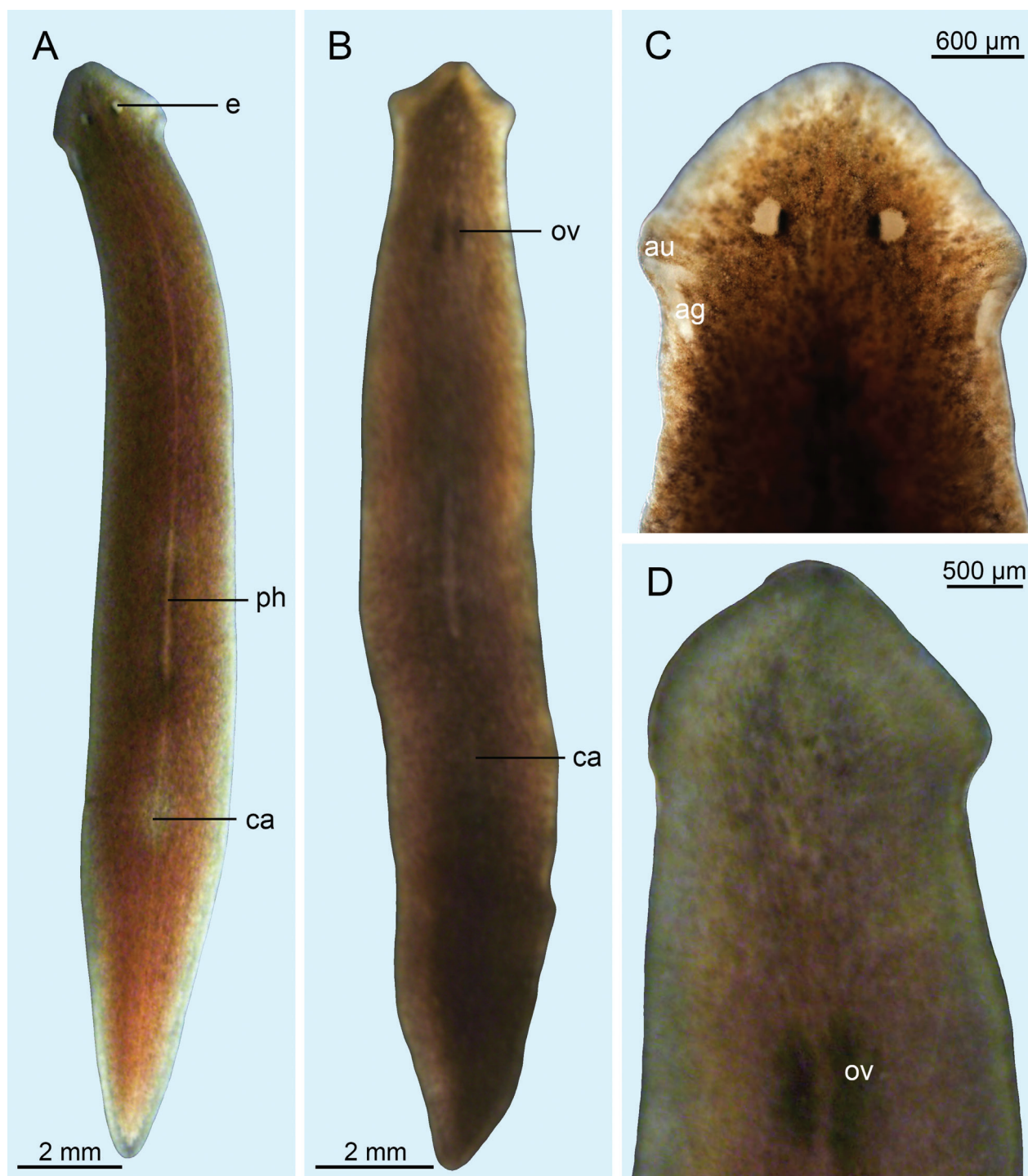
Figure 3. *Dugesia gemmulata*. **A.** Habitus of live, sexualised animal in dorsal view; **B.** Habitus of live, sexualised animal in ventral view; **C.** Anterior end, dorsal view; **D.** Anterior end, ventral view, showing ovaries.

apparatus, with the left oviduct opening into the common atrium and the right oviduct opening more dorsally into the vaginal section of the bursal canal (Figs 4E, 5C).

The large, irregularly egg-shaped copulatory bursa is situated immediately anterior to the penis bulb and is surrounded by a thin layer of intermingled longitudinal and circular muscle fibres (Figs 4C–F, 5). The bursal canal arises from the posterior surface of the copulatory bursa and runs caudally to the left of the copulatory apparatus,

subsequently communicating with the dorsal portion of the common atrium (Figs 4E, F, 5C, D). The bursal canal is lined by a nucleated, glandular epithelium, which is underlain by a subepithelial layer of longitudinal muscle fibres, followed by 2–5 layers of circular fibres. The coat of circular fibres on the ventral side of the bursal canal varies from 3–5 layers, while that on the dorsal side is thinner, being 2–3 layers thick. Furthermore, the ventral part of the most posterior section of the bursal canal, just
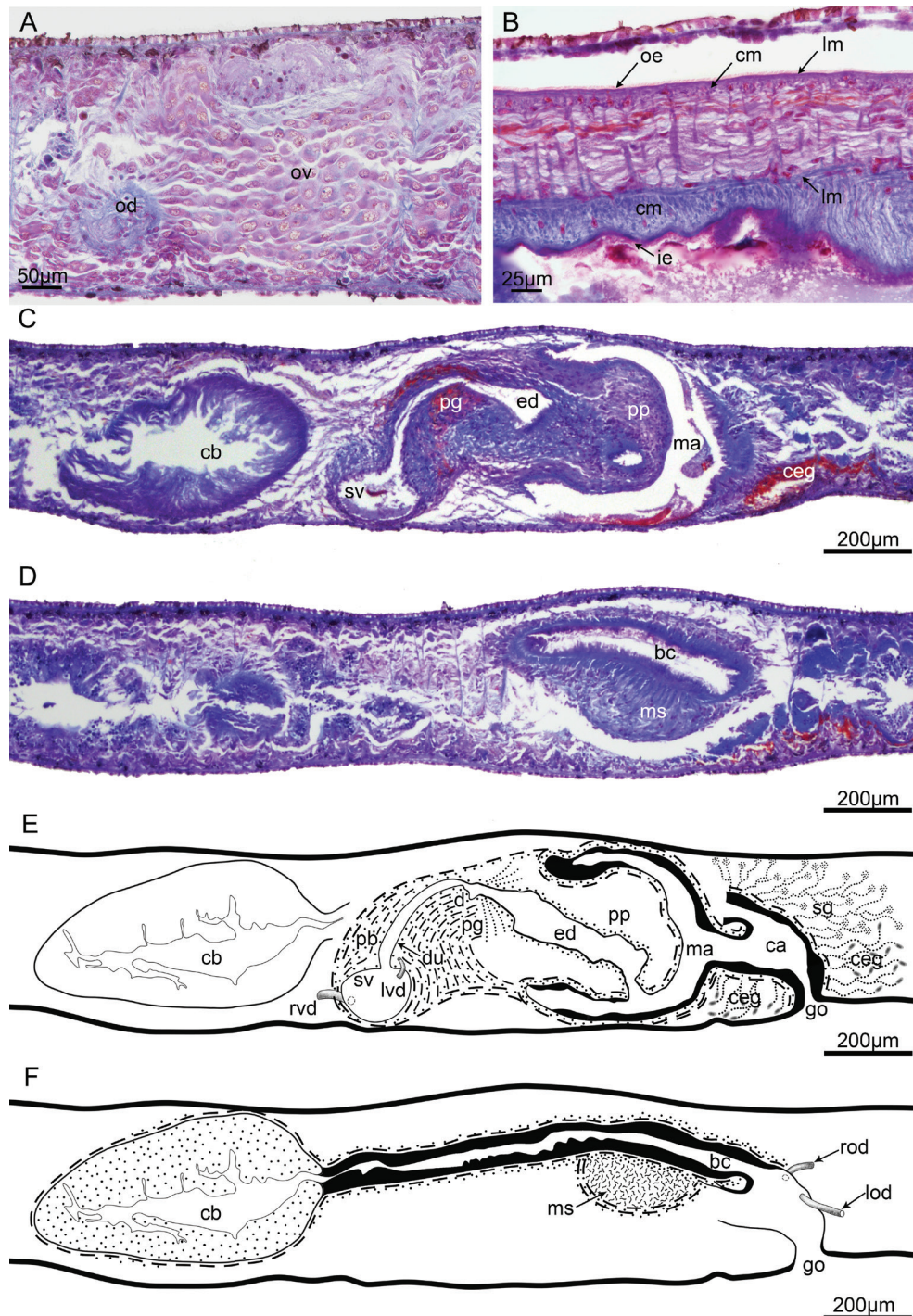
Figure 4. *Dugesia gemmulata*, holotype PLA-0101, sagittal sections and reconstructions of the copulatory apparatus. **A.** Photomicrograph showing ovaries and the opening of the oviduct; **B.** Photomicrograph showing musculature of the pharynx; **C.** Photomicrograph showing copulatory bursa, seminal vesicle, interconnecting duct, penis glands, ejaculatory duct, penis papilla, male atrium and cement glands; **D.** Photomicrograph showing bursal canal and muscular swelling; **E.** Reconstruction male copulatory apparatus; **F.** Reconstruction female copulatory apparatus.

anteriorly to its point of communication with the common atrium, carries a voluminous, ellipsoidal muscular swelling that measures about 348–481 µm in anterior-posterior direction (n = 3; Figs 4D, F, 5B, D, 6). The swelling consists of irregular, nucleated mesenchymal cells and is surrounded by a coat of intermingled muscles; there are also muscle fibres traversing the swelling in all directions in a more loosely arranged, irregular and reticulated way (Figs 4D, F, 5B, D, 6).

The male atrium is lined by an epithelium consisting of nucleated, cylindrical cells and is surrounded by a subepithelial layer of circular muscles, followed by 1–2 layers of longitudinal muscles. The male atrium communicates with the common atrium via a pronounced constriction
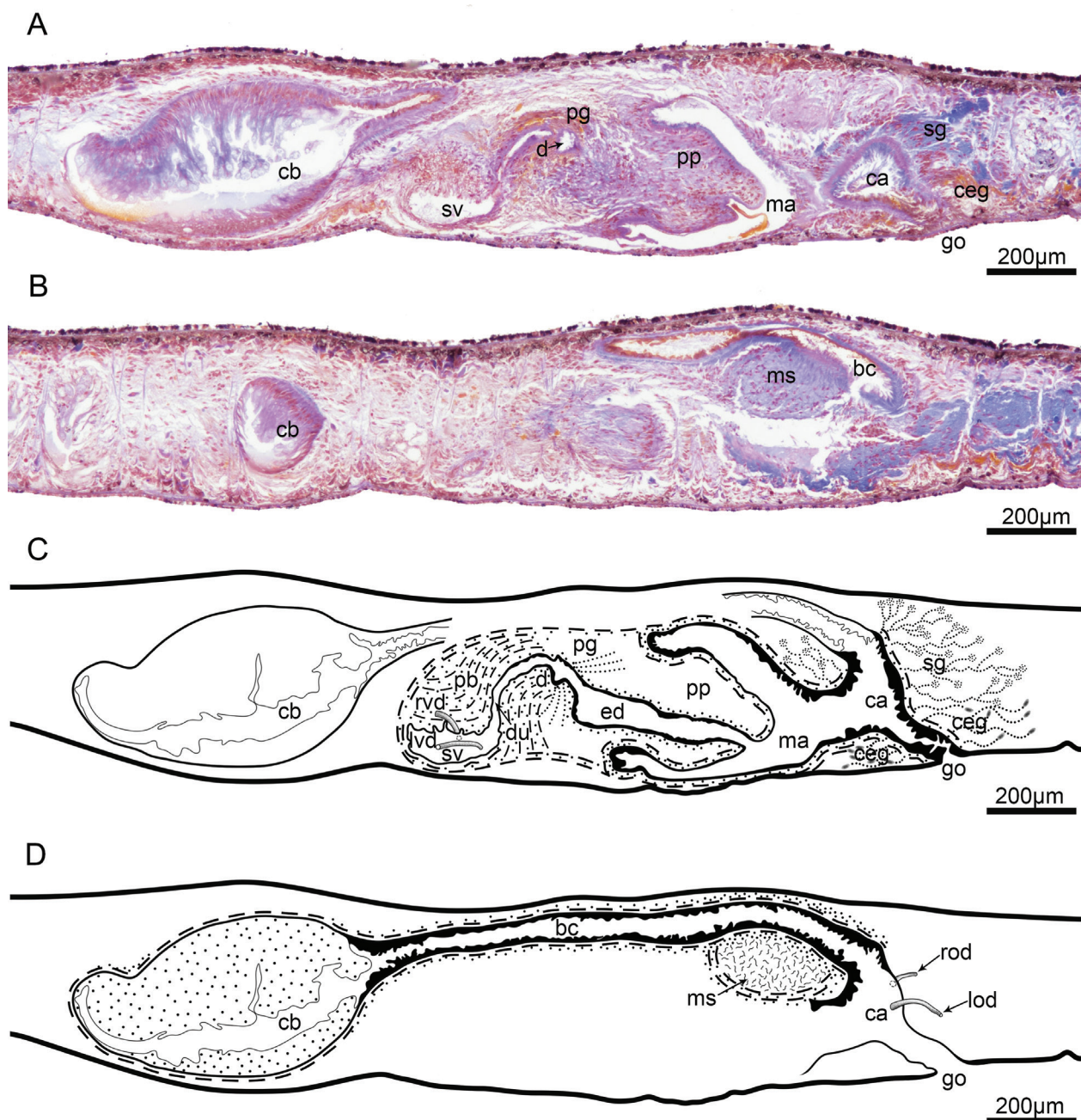
Figure 5. *Dugesia gemmulata*, paratype PLA-0102, sagittal sections and reconstructions of the copulatory apparatus. **A.** Photomicrograph showing copulatory bursa, seminal vesicle, diaphragm, penis glands, penis papilla, male atrium, common atrium, shell glands, cement glands and gonopore; **B.** Photomicrograph showing bursal canal and muscular swelling; **C.** Reconstruction male copulatory apparatus; **D.** Reconstruction female copulatory apparatus.

(Figs 4C–E, 5A, C, D). The common atrium is lined with an infranucleated epithelium, which is underlain by 1–2 layers of circular muscle, followed by a layer of longitudinal muscle. The common atrium opens ventrally through the gonopore, which is located at 1/3–1/4 of the body length (*n* = 3), as determined from the posterior body margin (Figs 4E, F, 5A, C, D).

Massive shell glands are distributed posteriorly to the common atrium and near the vaginal section of the bursal canal (Figs 4E, 5A, C). Near its opening into the common atrium, the bursal canal receives the cyanophilic secretion

of the shell glands (Figs 4E, 5A, C). Erythrophilic cement glands open into the ventral portion of the common atrium and into the gonoduct (Figs 4C, E, 5A, C).

Discussion

In our phylogenetic tree, the three individuals of *Dugesia gemmulata* occupy a single branch that shares a sister-group relationship with *D. umbonata* (Fig. 2). The long branch of *D. gemmulata* unequivocally indicates its high
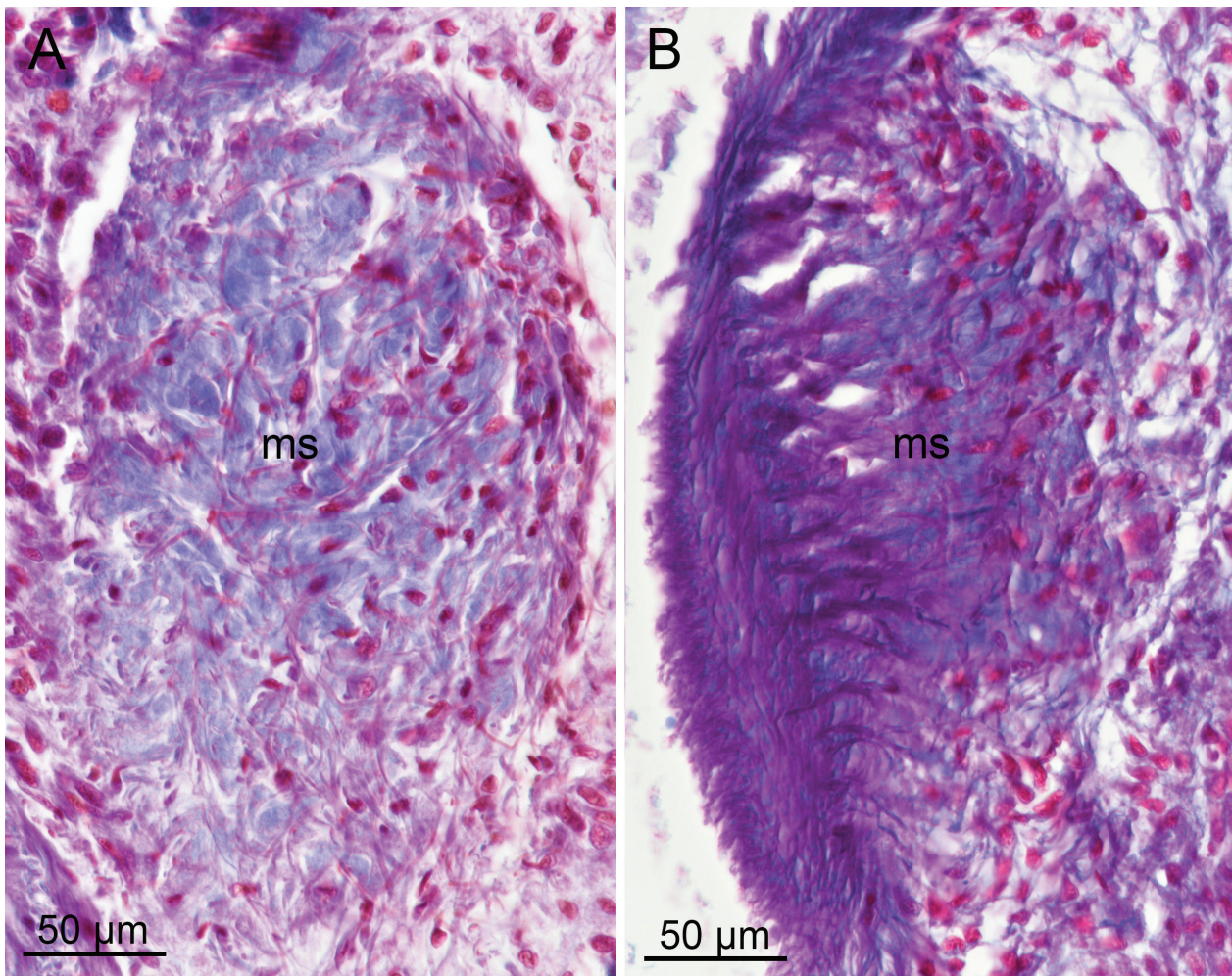
Figure 6. *Dugesia gemmulata*, paratype PLA-0103, horizontal sections. **A, B.** Photomicrographs showing the muscular swelling.

divergence from other species, while its phylogenetic position reveals that it belongs to a clade comprising other *Dugesia* species from the Australasian and Oriental regions. The topology of our phylogenetic tree (Fig. 2) basically corresponds with those generated in previous studies, except for some nodes.

The Australasian and Oriental clade is formed by three major branches that basically coincide with the topology of the trees of Song et al. (2020: figs 1, S2, S3) and Wang et al. (2021a, 2021b, 2022: figs 2). However, in the trees of Wang et al. (2021a, 2021b, 2022: figs 2), *D. japonica* clusters with the clade comprising *D. majuscula*, *D. verrucula* and *D. constrictiva*, whereas in our tree (Fig. 2) it forms a clade with *D. gemmulata* and *D. umbonata*. Similarly, in the tree of Song et al. (2020) *D. japonica* shares a sister-group relationship with *D. umbonata*. This discrepancy may be due to the different gene segments analysed by both ourselves and Song et al. (2020), i.e., complete mitochondrial genome (AB618487), while only a partial mitochondrial sequence (FJ646990) was used in Wang et al. (2021a, b, 2022).

Furthermore, the clade formed by the four species *D. deharvengi* Kawakatsu & Mitchell, 1989, *D. ryukyuensis* Kawakatsu, 1976, *D. batuensis* Ball, 1970,

and *D. notogaea* Sluys & Kawakatsu, 1998 receives only low support in our phylogenetic tree (0.60 pp; 70% bs), whereas this clade is robust in the trees of Song et al. (2020: fig. 1; 0.99 pp; 92% bs) and Wang et al. (2021a, 2021b, 2022: figs 2; 1.00 pp; 81% bs; 1.00 pp; 95% bs; 1.00 pp; 74% bs, respectively).

In our phylogenetic tree, a large clade comprising species from Cameroon, Western Palearctic, Australasian and Oriental regions is sister to a Madagascan clade, and together cluster with an Afrotropical and South-West Palearctic clade. This topology is the same as in Song et al. (2020: fig. 1), but differs from other trees in Song et al. (2020: figs S2, S3) and from those in Wang et al. (2021a, 2021b, 2022: figs 2) and Solà et al. (2022, figs 2, 3), in which the basal position is not taken by the Afrotropical and South-West Palearctic clade but by a Madagascan clade. However, in our tree the Madagascan clade comprises only three taxa, while the Afrotropical and South-West Palearctic clade contains only four OTUs. Thus, these two clades have only low representation, as compared to the other three major clades. Additionally, the node connecting the Madagascan group with the large clade comprising 35 species of *Dugesia* shows only rather low supporting values (0.61 pp; 66% bs), which may

contribute to the fact that the Madagascan group does not form the basal clade in our tree. Interestingly, in the analysis of Solà et al. (2022) it was shown that there are actually two Malagasy clades of which only one occupied a basal position in the phylogenetic tree.

Dugesia gemmulata exhibits an apomorphic feature that sets it immediately apart from all of its congeners, viz., the presence of a muscular swelling on the ventral side of its bursal canal. In contrast to *D. umbonata*, this muscular swelling is confined to the ventral side of the bursal canal, whereas in the former there is on the same posterior section of the bursal canal a structurally similar swelling or hump on the dorsal side of the duct. It is noteworthy that both species are characterised by the presence of a seminal vesicle that is located in the very antero-ventral section of the penis bulb and that from the dorsal wall of the vesicle arises a duct that shows a postero-dorsal loop before communicating with a small diaphragm. However, in *D. gemmulata* this loop is much more pronounced. In both species the oviducts open asymmetrically into the bursal canal. A clear difference between both species concerns the opening of the ejaculatory duct. *Dugesia gemmulata* exhibits a terminal or a subterminal ventral opening, whereas in *D. umbonata* the ejaculatory duct has a subterminal dorsal opening, the latter representing an apomorphic condition within the genus *Dugesia*. It is interesting that in the phylogenetic tree the sister-group relationship between *D. gemmulata* and *D. umbonata* is robust, thus strongly supporting their close affinity, which may explain the correlation between their anatomical characters, notably the presence of a muscular hump or swelling on the bursal canal.

Song et al. (2020) already argued that the muscular hump in *D. umbonata* is not homologous with the halo-like structure in the vaginal area of the bursal canal in *D. japonica*, which is also composed of mesenchymal tissue traversed by irregular muscle fibres. The same argument holds true for the non-homologous relationship between the ventral muscular swelling on the bursal canal of *D. gemmulata* and the halo-like structure in *D. japonica*.

Similar to the situation in *D. umbonata*, the sexualised specimens of *D. gemmulata* possessed hyperplasic ovaries and were devoid of testicular follicles, a condition that is not uncommon among such animals (cf. Song et al. 2020 and references therein).

Acknowledgements

References

Abascal F, Zardoya R, Telford MJ (2010) TranslatorX: Multiple alignment of nucleotide sequences guided by amino acid translations. Nucleic Acids Research 38(suppl 2): W7–W13. https://doi.org/10.1093/nar/gkq291

Chen Y-H, Chen X-M, Wu C-C, Wang A-T (2015) A new species of the genus *Dugesia* (Tricladida, Dugesiidae) from China. Zoological Systematics 40: 237–249.

Darriba D, Taboada GL, Doallo R, Posada D (2012) jModelTest2: More models, new heuristics and parallel computing. Nature Methods 9(8): 772. https://doi.org/10.1038/nmeth.2109

Edgar RC (2004) MUSCLE: Multiple sequence alignment with high accuracy and high throughput. Nucleic Acids Research 32(5): 1792–1797. https://doi.org/10.1093/nar/gkh340

Hoang DT, Chernomor O, von Haeseler A, Minh BQ, Vinh LS (2018) UFBoot2: Improving the ultrafast bootstrap approximation. Molecular Biology and Evolution 35(2): 518–522. https://doi.org/10.1093/molbev/msx281

Kalyaanamoorthy S, Minh BQ, Wong TKF, von Haeseler A, Jermiin LS (2017) ModelFinder: Fast model selection for accurate phylogenetic estimates. Nature Methods 14(6): 587–589. https://doi.org/10.1038/nmeth.4285

Kawakatsu M, Oki I, Tamura S (1995) Taxonomy and geographical distribution of *Dugesia japonica* and *D. ryukyuensis* in the Far East. Hydrobiologia 305(1–3): 55–61. https://doi.org/10.1007/BF00036363

Minh BQ, Schmidt HA, Chernomor O, Schrempf D, Woodhams MD, von Haeseler A, Lanfear R (2020) IQ-TREE 2: New models and efficient methods for phylogenetic inference in the genomic era. Molecular Biology and Evolution 37(5): 1530–1534. https://doi.org/10.1093/molbev/msaa015

Rambaut A, Drummond AJ, Xie D, Baele G, Suchard MA (2018) Posterior summarisation in Bayesian phylogenetics using Tracer 1.7. Systematic Biology 67(5): 901–904. https://doi.org/10.1093/sysbio/syy032

Ronquist F, Teslenko M, van der Mark P, Ayres DL, Darling A, Höhna S, Larget B, Liu L, Suchard MA, Huelsenbeck JP (2012) MrBayes 3.2: Efficient Bayesian phylogenetic inference and model choice across a large model space. Systematic Biology 61(3): 539–542. https://doi.org/10.1093/sysbio/sys029

Sluys R, Riutort M (2018) Planarian diversity and phylogeny. In: Rink JC (Ed.) Planarian Regeneration: Methods and Protocols. Methods in Molecular Biology (Vol. 1774). Humana Press, Springer Science+Business Media, New York, 1–56. https://doi.org/10.1007/978-1-4939-7802-1_1

Solà E, Leria L, Stocchino GA, Bagherzadeh R, Balke M, Daniels SR, Harrath AH, Khang TF, Krailas D, Kumar B, Li M-H, Maghsoudlou A, Matsumoto M, Naser N, Oben B, Segev O, Thielicke M, Tong X, Zivanovic G, Manconi R, Baguñà J, Riutort M (2022) Three dispersal routes out of Africa: The puzzling biogeographical

history in freshwater planarians. Journal of Biogeography 49(7): 1219–1233. https://doi.org/10.1111/jbi.14371

Song X-Y, Li W-X, Sluys R, Huang S-X, Li S-F, Wang A-T (2020) A new species of *Dugesia* (Platyhelminthes, Tricladida, Dugesiidae) from China, with an account on the histochemical structure of its major nervous system. Zoosystematics and Evolution 96(2): 431–447. https://doi.org/10.3897/zse.96.52484

Talavera G, Castresana J (2007) Improvement of phylogenies after removing divergent and ambiguously aligned blocks from protein sequence alignments. Systematic Biology 56(4): 564–577. https://doi.org/10.1080/10635150701472164

Wang L, Dong Z-M, Chen G-W, Sluys R, Liu D-Z (2021a) Integrative descriptions of two new species of *Dugesia* from Hainan Island, China (Platyhelminthes, Tricladida, Dugesiidae). ZooKeys 1028: 1–28. https://doi.org/10.3897/zookeys.1028.60838

Wang L, Chen J-Z, Dong Z-M, Chen G-W, Sluys R, Liu D-Z (2021b) Two new species of *Dugesia* (Platyhelminthes, Tricladida, Dugesiidae)

from the tropical monsoon forest in Southern China. ZooKeys 1059(3): 89–116. https://doi.org/10.3897/zookeys.1059.65633

Wang L, Wang Y-X, Dong Z-M, Chen G-W, Sluys R, Liu D-Z (2022) Integrative taxonomy unveils a new species of *Dugesia* (Platyhelminthes, Tricladida, Dugesiidae) from the southern portion of the Taihang Mountains in northern China, with the description of its complete mitogenome and an exploratory analysis of mitochondrial gene order as a taxonomic character. Integrative Zoology. Online version. https://doi.org/10.1111/1749-4877.12605

Xia X, Zheng X, Salemi M, Chen L, Wang Y (2003) An index of substitution saturation and its application. Molecular Phylogenetics and Evolution 26(1): 1–7. https://doi.org/10.1016/S1055-7903(02)00326-3

Yang Y, Li J-Y, Sluys R, Li W-X, Li S-F, Wang A-T (2020) Unique mating behavior, and reproductive biology of a simultaneous hermaphroditic marine flatworm (Platyhelminthes, Tricladida, Maricola). Invertebrate Biology 139(1): e12282. https://doi.org/10.1111/ivb.12282